Supporting Information

When Hydrophobicity Meets Strong Interactions to Capture Highly Polar Volative Organic Compounds

Maria Inês Severino,[a,e] Abeer Al Mohtar,[b,e] Carla Vieira Soares,[c,e] Oleksii Kolmykov,[a] Cátia Freitas,[b] Iurii Dovgaliuk,[a] Charlotte Martineau,[d] Vanessa Pimenta,[a] Farid Nouar,[a] Guillaume Maurin*,[c] Moisés L. Pinto*,[b] Christian Serre [a]*

[a.] *Institut des Matériaux Poreux de Paris (IMAP), ESPCI Paris, Ecole Normale Supérieure, CNRS, PSL University, 75005 Paris, France ; E-mail: christian.serre@espci.psl.eu*

[b.] *CERENA, Departamento de Engenharia Química, Instituto Superior Técnico, Universidade de Lisboa, 1049-001 Lisboa, Portugal. Email : moises.pinto@tecnico.ulisboa.pt*

[c.] *ICGM, Univ. Montpellier, CNRS, ENSCM, Montpellier 34293, France ; Email : guillaume.maurin1@umontpellier.fr*

[d.] *Institut Lavoisier de Versailles (ILV), Université de Versailles St Quentin (UVSQ), 45 avenue des Etats-Unis, 78035 Versailles, France*

[e.] *These authors contributed equally: Maria Inês Severino, Abeer Al Mohtar, Carla Vieira Soares*

† Footnotes relating to the title and/or authors should appear here.
Electronic Supplementary Information (ESI) available: [details of any supplementary information available should be included here]. See DOI: 10.1039/x0xx00000x

1. *Experimental*

1.1 Molecular simulations

Periodic DFT calculations for both empty and acetic acid loaded MIL-53(Al)-nCF_3 (n=1,2) were carried out with the Quantum-Espresso package [1] [2]. A plane wave basis set was used to expand the one-electron Kohn-Sham orbitals, with a kinetic energy cutoff of 60 Ry (480 Ry for the charge density). The ion cores were described by Vanderbilt ultrasoft pseudopotentials [3] and the integration in the first Brillouin zone was performed at the Γ-point. The atomic positions and the cell parameters of the empty LP and NP MIL-53(Al)-nCF_3 structures were relaxed by minimizing the total energy gradient until the force components were lower than 0.001 Ry $Bohr^{-1}$. All the geometry optimizations were performed with the PBE functional where the dispersion correction was treated with the DFT-D2 method [4]. The DFT optimized structures along their unit cell parameters are reported in Figure S1 and Table S1.

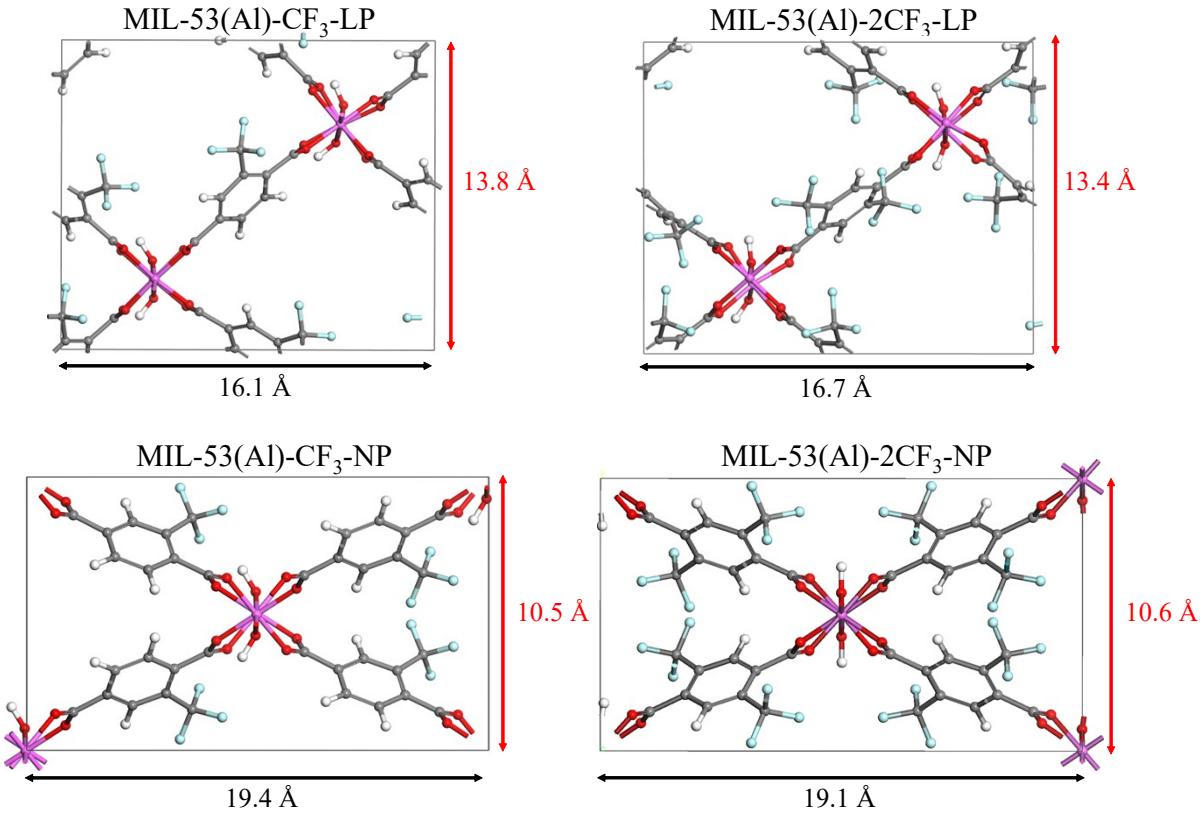

Figure S1 - DFT optimized structures of MIL-53(Al)-CF_3–LP, MIL-53(Al)-2CF_3-LP, MIL-53(Al)-CF_3-NP and MIL-53(Al)-2CF_3-NP. Color code: pink – Al; red – O; grey – C; blue – F.

Table S1 - DFT optimized cell parameters for the MIL-53(Al)-CF_3–LP, MIL-53(Al)-2CF_3-LP, MIL-53(Al)-CF_3-NP and MIL-53(Al)-2CF_3-NP crystal structures.

MOF	**MIL-53(Al)-CF_3-LP**	**MIL-53(Al)-CF_3-NP**	**MIL-53(Al)-2CF_3-LP**	**MIL-53(Al)-2CF_3-NP**

a (Å)	16.1	19.4	16.6	19.1
b (Å)	6.7	6.6	6.9	6.7
c (Å)	13.8	10.5	13.4	10.2
β (deg.)	89.7	109.9	88.7	108.3
V (Å³)	1488.1	1269.8	1510.1	1244.6

The interactions energies for the acetic acid-loaded MIL-53(Al)-CF_3-LP, MIL-53(Al)-CF_3-NP and MIL-53(Al)-2CF_3-LP structures containing 1 acetic acid molecule per unit cell were calculated according to the equation below:

$$\text{Interaction Energy} = E_{(\text{MOF/acetic acid})} - [E_{(\text{acetic acid})} + E_{(\text{MOF})}]$$

The geometry optimized geometries for the acetic acid loaded MOFs are reported in Figure S2.

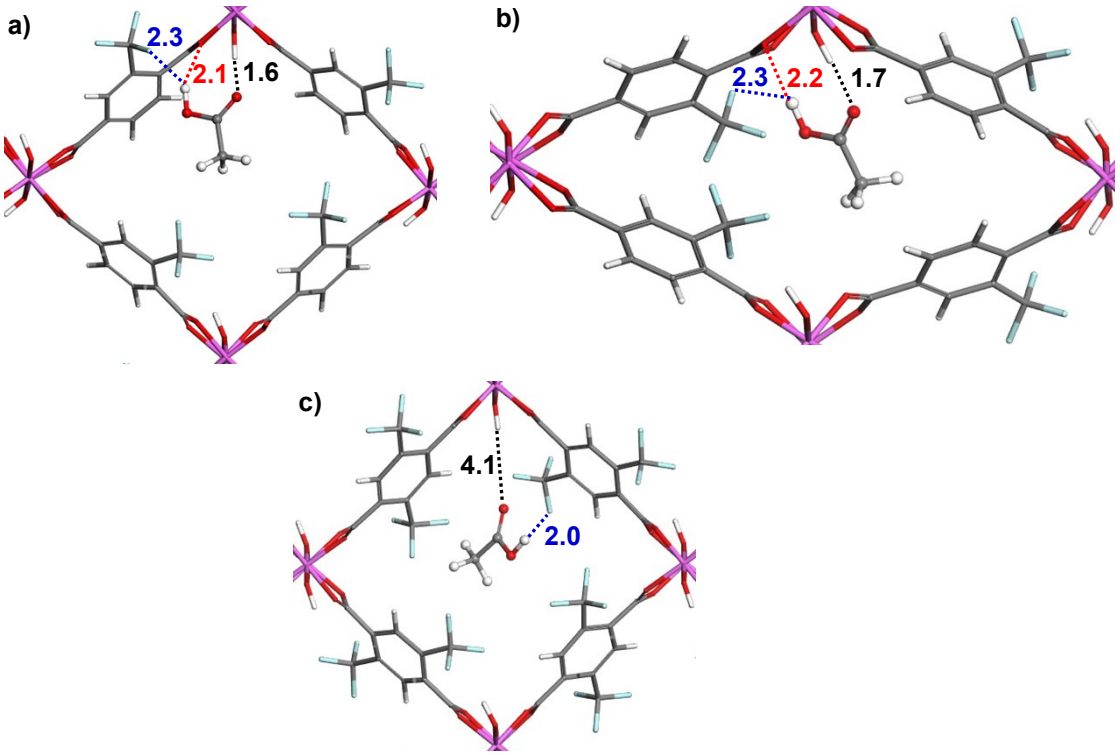

Figure S2 - DFT optimized structures of the acetic acid loaded MIL-53(Al)-CF_3–LP, MIL-53(Al)-2CF_3-LP, and MIL-53(Al)-CF_3-NP. Color code: pink – Al; red – O; grey – C; blue – F. The main distances involved in the adsorption process, O_CO($H_4C_2O_2$)–H(μ-OH) in black, H_OH($H_4C_2O_2$)–F in blue and H_OH($H_4C_2O_2$)–O(COO^-) in red are expressed in Å.

Dynamic adsorption characterization of MIL-53(Al)-CF_3 in a packed bed was tested in a setup similar to the one shown in Figure S3 of a paper published by Sayari group[5]. Where, a flow of gases was controlled using mass flow meters (Stainless Steel Gas Thermal Mass Flow-Controller, McMillan 80SD), and the path of gases was controlled by 4-way valves.

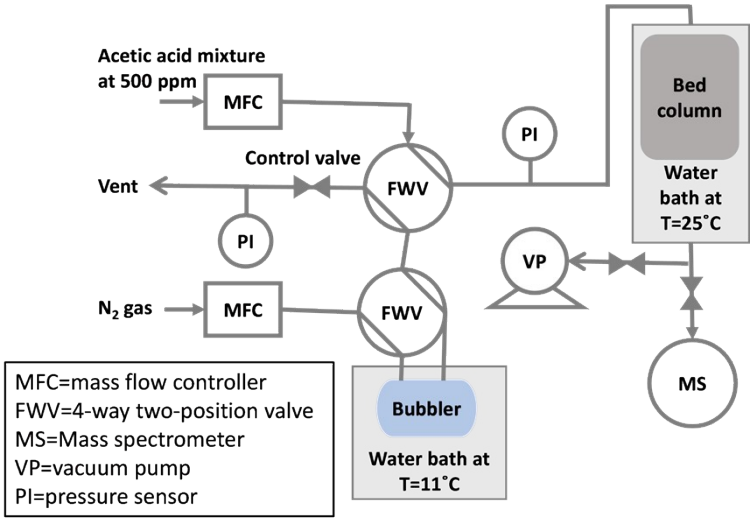

Figure S3 - Schematic diagram of breakthrough.

Temperature-programmed desorption was done in a set-up adapter from the one of the Breakthrough. Around 25 mg of activated sample (T=150 °C D= 15 hours) was loaded inside a stainless steel column of inner diameter of 6.4 mm. The sample was activated in-situ using a flow of nitrogen of 40 cm^3 min^{-1} for 1 hour under temperature of 150 °C (labmade electric oven equipped with Eurotherm controller, PV accuracy <0.25%, heating ramp 5 °C min^{-1}). The column was immersed in a water bath at temperature of 25 °C (water bath VWR, accuracy 0.1 °C). The pressure of the column as well as the vent pressure were monitored using pressure sensors and were maintained at equal pressure close to atmospheric pressure. The sample was then left to equilibrate with moisture controlled at around 40% by passing the flow of nitrogen through a bubbler of water kept at 11 °C (water bath VWR, accuracy 0.1 °C).

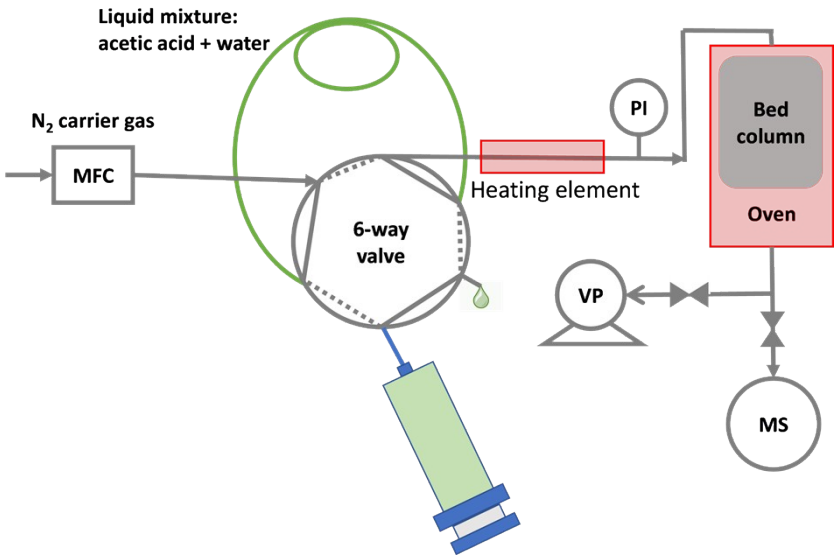

Figure S4 - Schematic diagram of TPD experimental setups.

2. *Results:*

2.1. MIL-53(Al)-*n*CF_3 (*n*= 1,2) - Hydrothermal synthesis

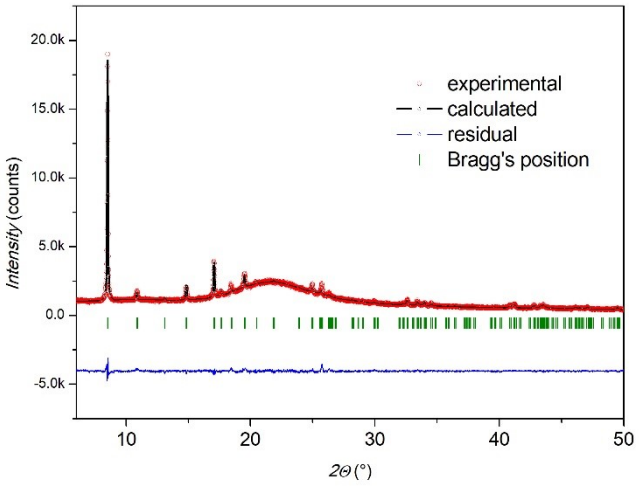

Figure S5 – Refinement plot for MIL-53(Al)-CF_3 (LP) crystal structure using Cu Kα radiation and Rietveld method (space group *Imma*): *a* = 16.255(2), *b* = 6.6484(6), *c* = 13.4984(13) Å; R_I = 10.00 %.

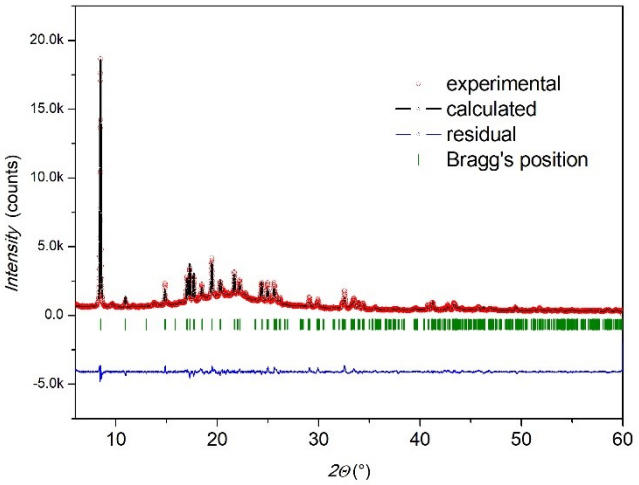

Figure S6 – Refinement plot for MIL-53(Al)-2CF_3 (LP) crystal structure using Cu Kα radiation and Rietveld method (space group *Pnna*): *a* = 16.1757(9), *b* = 6.6339(4), *c* = 13.6279(7) Å; R_I = 5.23 %.

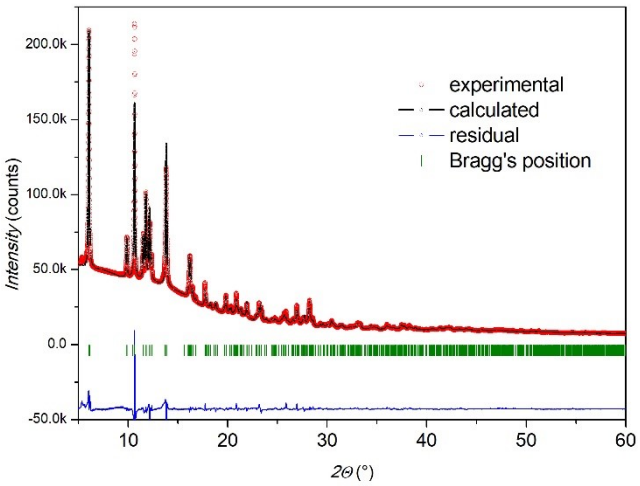

Figure S7 – Refinement plot for MIL-53(Al)-2CF_3 (NP) crystal structure using synchrotron radiation (SOLEIL (France), λ = 0.970816 Å) and Rietveld method (space group *C*2/*c*): *a* = 18.9966(5), *b* = 10.6421(3), *c* = 6.6467(2) Å, *β* = 108.622(2)°; R_I = 6.58 %.

Table S2 – The interatomic distance and angle constraints used for the crystal structure refinement of MIL-53(Al)- *n*CF_3 (*n* = 1, 2)

Atoms 1	**Atom 2**	**Atom 3**	**Distance, Å**	**Sigma, Å**	**Angle, °**	**Sigma, °**
Al–	O		1.90	0.03		
C=	O		1.28	0.001		
C–	C		1.51	0.001		
C=	C		1.40	0.001		
C–	F		1.38	0.001		
F	F		2.20	0.001		
O=	C=	O			120.0	0.1
O=	C–	C			120.0	0.1
C–	C=	C			120.0	0.1
C=	C=	C			120.0	0.1
C–	C–	F			109.5	0.1
F–	C–	F			109.5	0.1

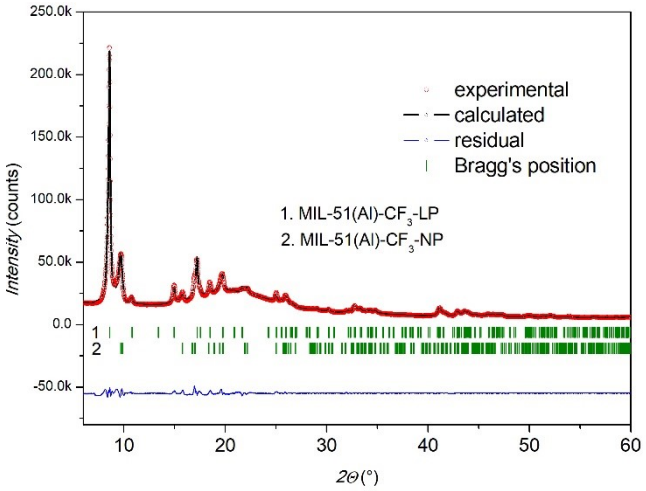

Figure S8 – Le-Bail refinement plot for the LP and NP polymorphs mixture from MIL-53(Al)-CF_3 using Cu Kα radiation: LP, space group *Imma*: a = 16.4064, b = 6.6209, c = 13.2201 Å; NP, space group *C2/c*: a = 18.9289, b = 10.5943, c = 6.6358 Å, β = 108.43°; R_I = 0.3 %.

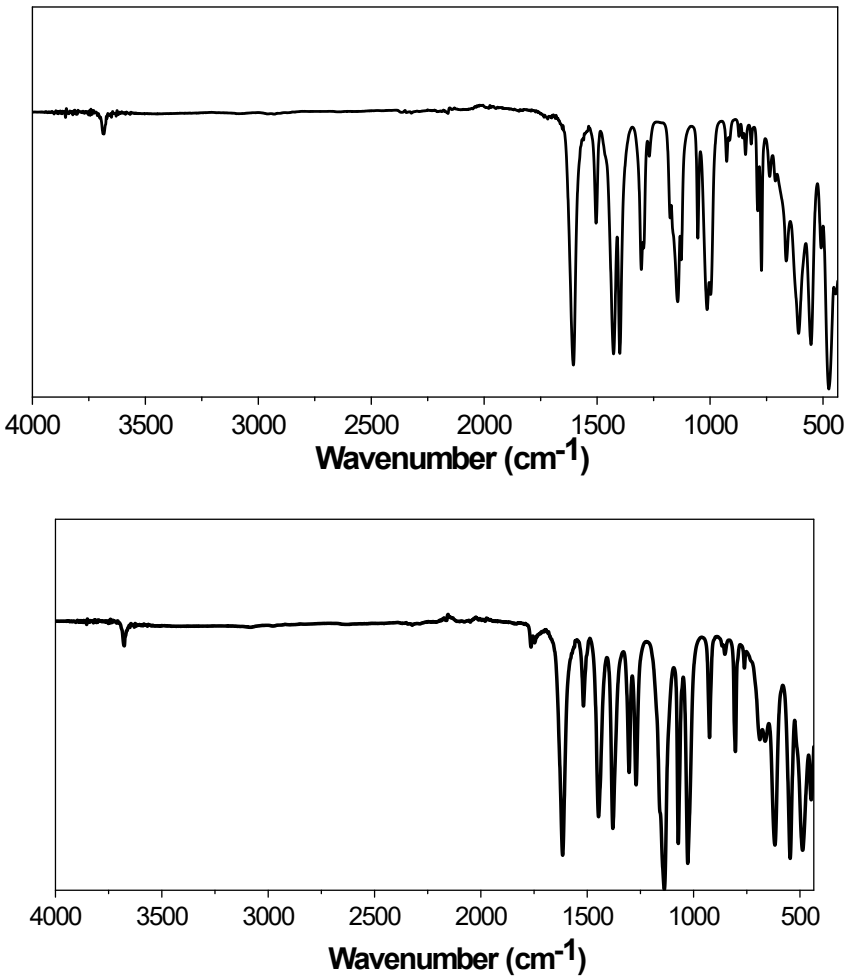

Figure S9 – Transmission IR spectra of (a) MIL-53(Al)-CF_3 and (b) MIL-53(Al)-$2CF_3$.

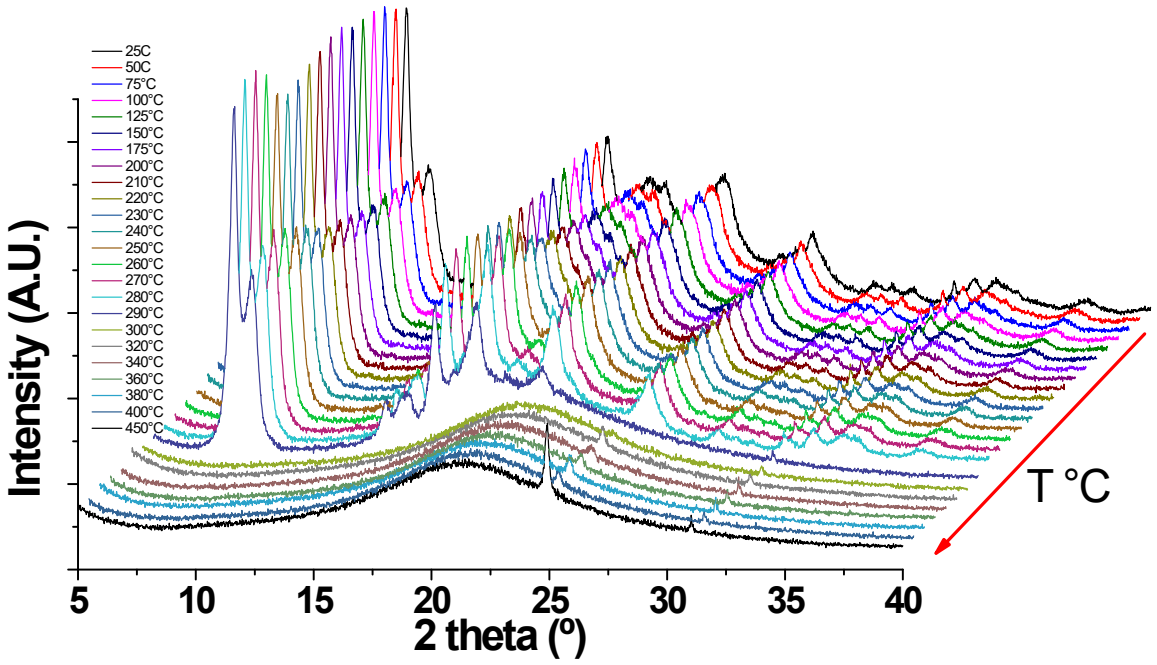

Figure S10 – Variable-Temperature X-ray powder diffraction of MIL-53(Al)-2CF_3 (CuKα radiation, λ = 1.5418 Å).

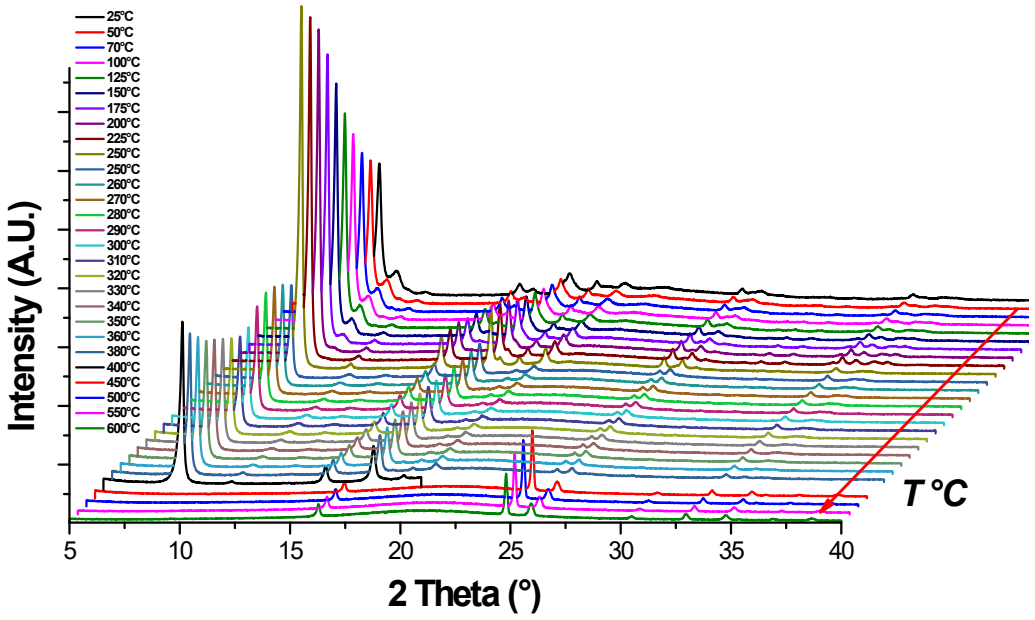

Figure S11 – Variable-Temperature X-ray powder diffraction of MIL-53(Al)-CF_3 (CuKα radiation, λ = 1.5418 Å).

Two weight-loss steps are visible in the thermogravimetric spectrum (Figure S12 and Figure S13) the first slight step before 100 °C is due to traces of free solvent. The second weight loss after 350 °C corresponds to linker decomposition, resulting in the total decomposition of the organic compounds into Al_2O_3. The different weight losses of each TGA are specified in Figure S12 and Figure S13.

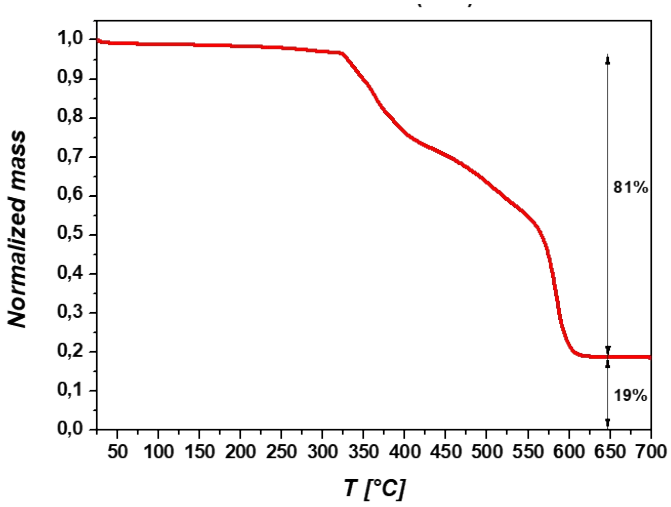

Figure S12 – TGA curve (5 °C per min under O_2) of as synthesized MIL-53(Al)-CF_3.

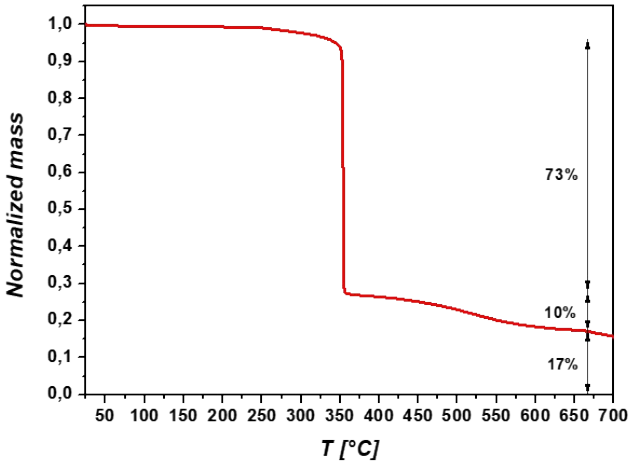

Figure S13 – TGA curve (5 °C per min under O_2) of as synthesized MIL-53(Al)-$2CF_3$.

Table S3 – The phase analysis and the corresponding unit cell parameters of MIL-53(Al)- nCF_3 (n = 1, 2) samples at various conditions

Solvent	S.G.	a (Å)	b (Å)	c (Å)	β (deg.)	V (Å^3)
			MIL-53(Al)-CF_3			

hydrated	C2/c	18.928	10.594	6.635	108.429	1262.474
(air)	Imma	16.406	13.220	6.6209		1436.053
Dry	C2/c	18.928	10.594	6.6357	108.429	1262.474
(air)	Imma	16.406	13.220	6.620		1436.053
Ethanol	Imma	16.477	13.238	6.622		1444
Acetic acid	Imma	16.124(2)	13.639(2)	6.6476(7)		1462
			MIL-53(Al)-2CF$_3$			
AS	Pnna	16.1759(9)	6.6340(4)	13.6276(7)		1476
hydrated	C2/c	18.900(2)	6.6219(6)	10.6232(9)	108.55(1)	1260
(air)	Pnna	15.95371	6.64866	13.41601		1423
Ethanol	Pnna	16.18630	6.63846	13.61196		1462.634
Acetic acid	Pnna	16.058(2)	6.6358(6)	13.728(1)		1462
	P 2_1/n	19.915(8)	6.6219(6)	10.465(2)	108.75(9)	1315

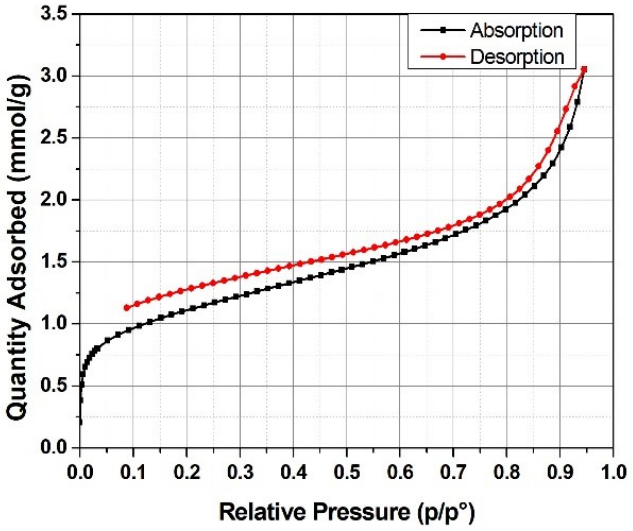

Figure S13 – The nitrogen adsorption isotherm, at 77 K, of MIL-53(Al)-CF_3.

2.2. Grand canonical Monte Carlo simulations

Grand canonical Monte Carlo simulations were further performed at 298 K to evaluate the saturation uptake of acetic acid in both MIL-53(Al)-CF_3–LP, MIL-53(Al)-2CF_3-LP.The MOF frameworks were treated as a charged Lennard-Jones (LJ) interacting site with LJ parameters taken from Universal Force Field (UFF) [6] and DREIDING [7] force field for the description of all atoms of the inorganic and the organic nodes respectively. The partial charges were extracted from periodic Density Functional Theory (DFT) calculations using the restrained electrostatic potential (RESP) method [8]. In this work the model reported by Kamath et al.[9] was adopted to described acetic acid. The LJ cross parameters corresponding to the interactions between the guest and the MOF framework were obtained using the Lorentz−Berthelot mixing rules. For each state point, 2x10^8 Monte Carlo steps have been used for

both equilibration and production runs. In addition to this, we analyzed the preferential distribution of the acetic acid molecules coupled with the Radial Distribution Functions (RDF) plot for the acetic acid/MOF pairs averaged over the $2x10^8$ Monte Carlo production steps.

2.2 MIL-53(Al)-*n*CF3 (*n*= 1,2) – Reflux synthesis

MIL-53(Al)-xCF_3 were initially synthesized in 25 mL scale under reflux in a green solvent. To prove the scalability and the MOF performance MIL-53(Al)-CF_3-LS was produced at a 2000 mL scale. The mixture of aluminum chloride hexahydrated, 2- (Trifluoromethyl)terephthalic acid/2,5-bis(trifluoromethyl)terephthalic and sodium hydroxide in a 3 : 2 : 4 molar ratio was refluxed in 1250 mL of water overnight. The solid was recovered by centrifugation and washed with ethanol. A white powder was obtained after drying at 150°C for 16 hours under primary vacuum. The PXRD patterns of MIL-53(Al)- *n*CF_3 are similar to the one of the smaller scale sample; it corresponds mainly to the LP (Figure S14).

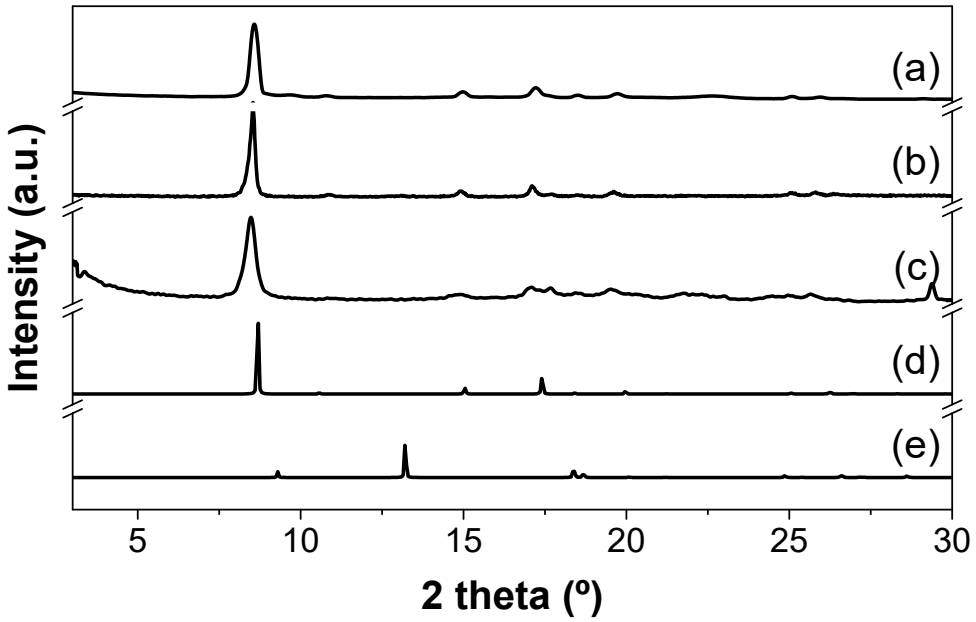

Figure S14 - Experimental PXRD pattern of (a) MIL-53(Al)-CF_3-LS, (b) MIL-53(Al)-CF_3 in 25 mL scale, (c) MIL-53(Al)-$2CF_3$, compared with theoretical patterns of the two different pores configuration, (d) Large pore (LP) and (e) narrow pore (NP) (CuKα radiation, λ = 1.5418 Å).

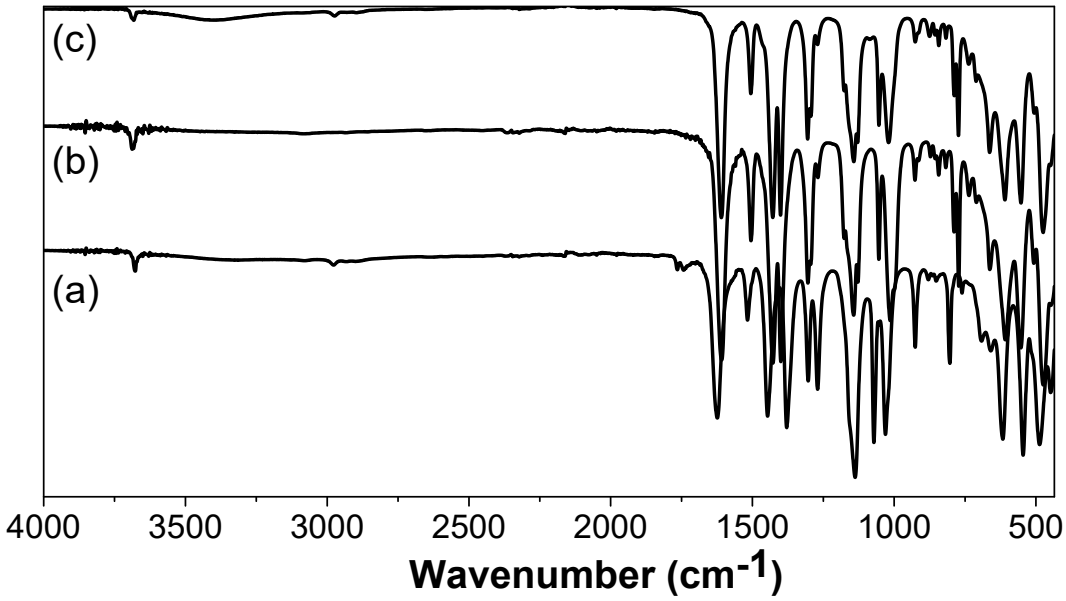

Figure S15 - Shows the IR spectra of MIL-53(Al)- *n*CF_3 series, (a) MIL-53(Al)-CF_3-LS, (b) MIL-53(Al)-CF_3 in 25 mL scale, (c) MIL-53(Al)-$2CF_3$. The presence of the characteristic bands of MIL-53(Al) was confirmed. It can be observed that the transmission IR spectrum of product showed no traces of free acid (original band ν C=O at 1760 cm^{-1}).

Two weight-loss steps are visible in the thermogravimetric spectrum (Figure S16). the first one before 100°C is due to traces of free water. The second weight loss at 350 - 600°C corresponds to linker decomposition, resulting in the total decomposition of the organic compounds into Al_2O_3. The different weight losses of each TGA are specified in Figure S16.

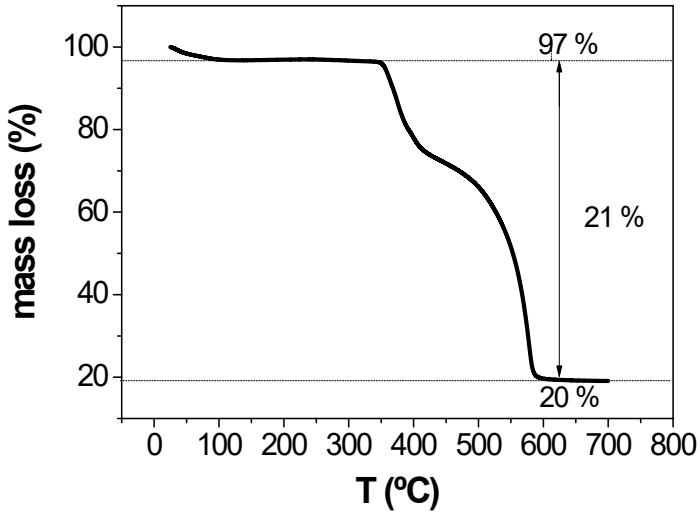

Figure S16 - TGA curve (5°C per min under O_2) of MIL-53(Al)-CF_3-LS.

N_2 sorption isotherm is presented in Figure S17, the Brunauer–Emmett–Teller (BET) surface area of MIL-53(Al)-CF_3-LS was calculated to be 780 $m^2\ g^{-1}$, similar to the surface area obtained for the MOF synthesized in small scale, 720 $m^2\ g^{-1}$. MIL-53(Al)-$2CF_3$ was much lower with the calculated surface area of 265 $m^2\ g^{-1}$

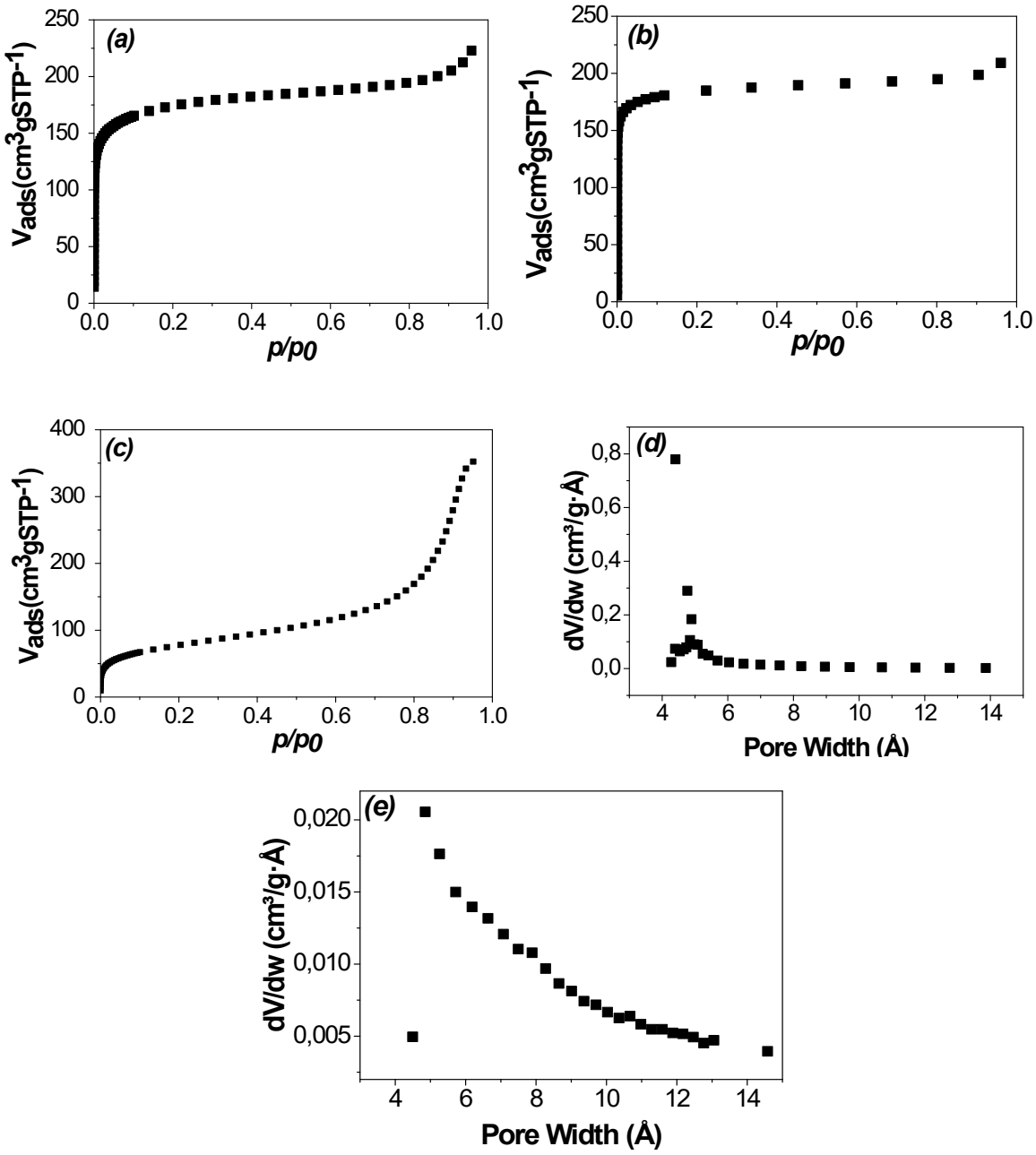

Figure S17 - Nitrogen adsorption isotherms, at 77K of (a) MIL-53(Al)-CF_3 in 25 mL, (b) MIL-53(Al)-CF_3 in 2 L scale, (c) MIL-53(Al)-$2CF_3$, and pore size distribution calculated using the Horvath–Kawazoe method for (d) MIL-53(Al)-CF_3 in 2 L scale, (e) MIL-53(Al)-$2CF_3$.

Acetic acid dynamic adsorption

The region of interest of the typical acetic acid concentrations found in museums (which varies greatly but remains in the ppb/ppm region):

$$C = \frac{C(ppm)}{V_M \times 10^6} = 2.07833 \times 10^{-8}\ (mol\ cm^{-3}) \quad (1)$$

Where $V_M = 24000$ cm³ is the molar volume at *T* = 25 ˚C and atmospheric pressure.

The adsorbed volume (cm³) was calculated by:

$$V_{ads} = V_{sample} - V_{background} \quad (2)$$

Where V_{sample} is obtained by considering the acetic acid flowrate (cm³/min) multiplied by the time of the experiment, then deducting the left out amount by integrating the area under the curve, of the signal acquired by the mass spectrometer as function of time, upon setting the maximum signal to the flowrate used (52 cm³/min). $V_{background}$ is obtained upon repeating the same procedure for the background measurement (with an empty column). The calculated adsorbed volume corresponding to the measurement shown in Figure 3 is 5.15x10³ cm³. The dynamic adsorbed quantity is obtained upon multiplying the adsorbed volume by the concentration. Taking into consideration the mass of the sample used of 25 mg:

$$n_{ads} = \frac{V_{ads} \times C}{m_{sample}} = 3.82\ mmol\ g^{-1} \quad (3)$$

To compare the amount dynamically adsorbed in the presence of moisture with the amount adsorbed in equilibrium for a clean sample, the concentration of acetic acid needs to be converted to partial pressure. This can be achieved by using the non-ideal gas law:

$$p = (\frac{n}{V})ZRT \quad (4)$$

With p the pressure, $(\frac{n}{V})$ the concentration, *R* the gas constant and *T* the temperature in *K* and *Z* the gas compressibility factor *Z*, expressed as function of p (in Pa) as[10]:

$$Z = 0.351 + 0.729p^{-0.176} \quad (5)$$

The calculated pressure for the used concentration using the ideal gas law is $p_{ideal} =$ 51.5 Pa. This gives *Z* = 0.715 and $p = Z \times p_{ideal}$=36.83 Pa. The saturation pressure of acetic acid at 25 °C and atmospheric pressure is 2118.36 Pa, thus, $p/p_o = 0.0174$.

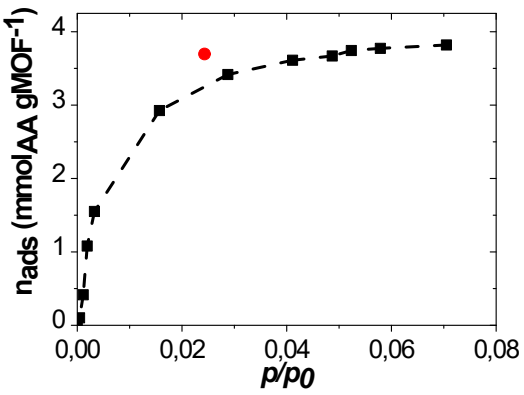

Figure S18 - Acetic acid adsorption isotherms at T = 25 °C (■) with the value obtained from the breakthrough indicated (●).

NMR results

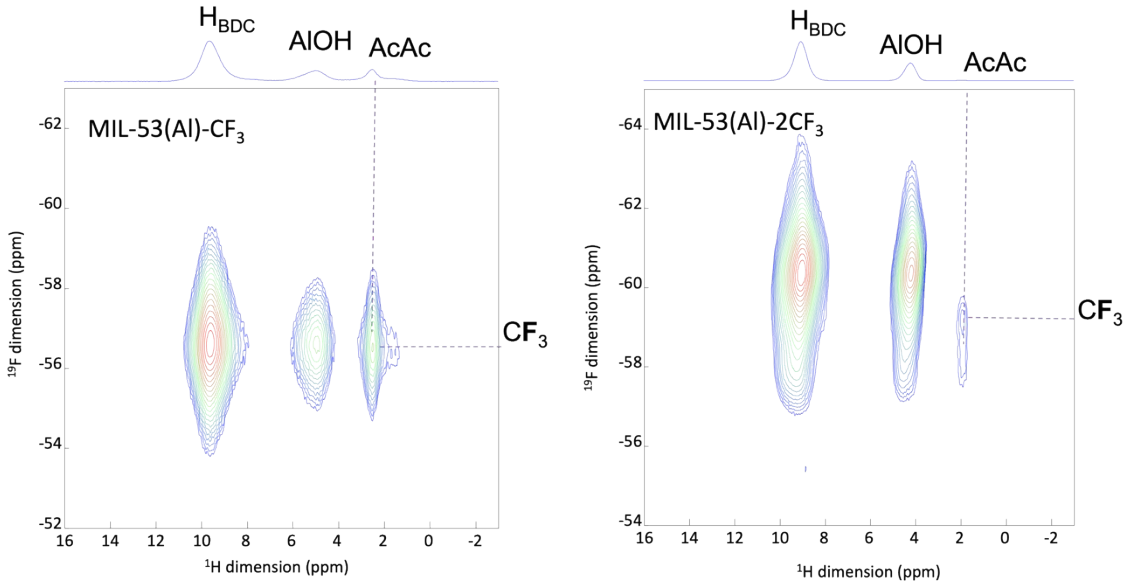

Figure S19 - ^{1}H-^{19}F 2D MAS NMR spectra of MIL-53(Al)-CF_3 (left) and MIL-53(Al)-$2CF_3$ (right). The dash lines show the correlation between the ^{19}F of the CF_3 groups and the protons of the acetic acid molecules (AcAc).

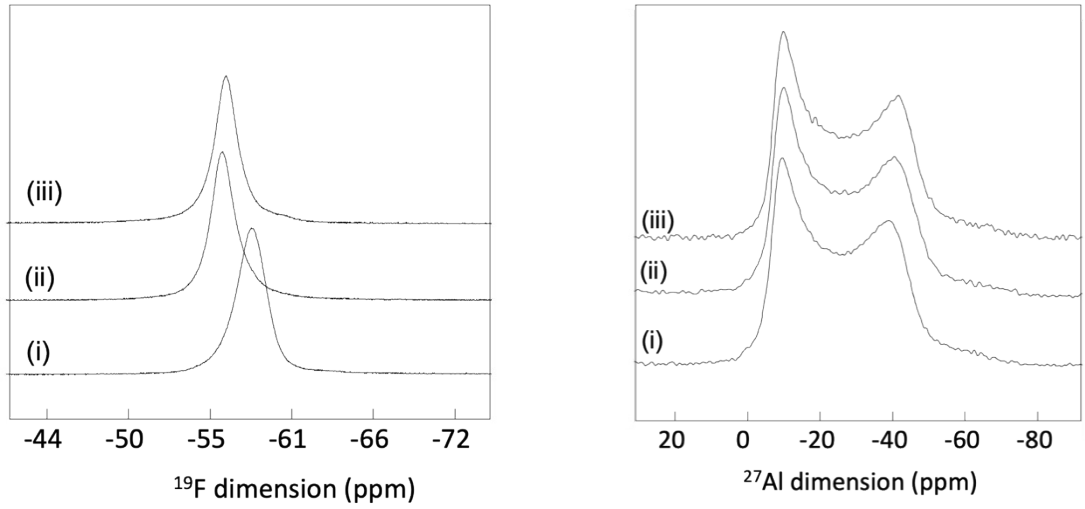

Figure S20 - ^{19}F (left) and ^{27}Al (right) NMR spectra of MIL-53(Al)-CF_3 recorded on (i) the activated sample, (ii) the activated sample exposed to acetic acid, (iii) the activated sample exposed to acetic acid in presence of moisture.

Temperature-programmed desorption

25 mg of activated MIL-53(Al)-CF3 was loaded in the column of inner diameter of 6.4 mm. The sample was activated in-situ and then left to equilibrate with moisture controlled at around 40 %RH. The flow

of gas was switched to the acetic acid mixture while the output of the column is recorded by the mass spectrometer (Prismapro, Pefeiffer).

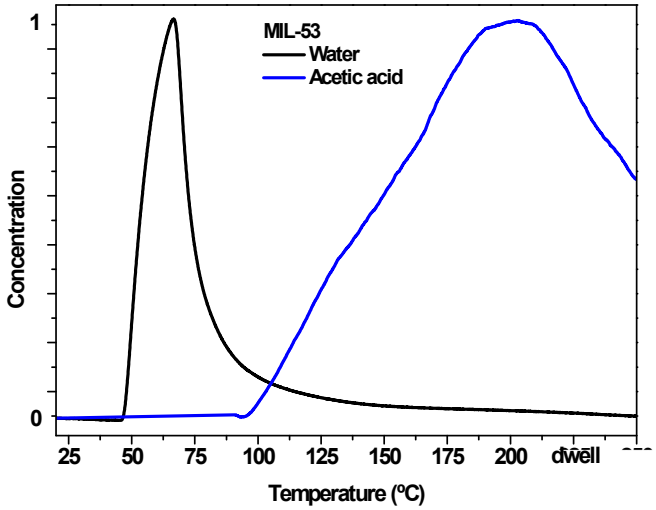

Figure S21 - TPD measurement on MIL-53(Al), after adsorption of water and acetic acid mixture.

1.2 MIL-53(Al)

MIL-53(Al) was typically synthesized under reflux. In a typical synthesis 15 mmol (3.62 g) of $AlCl_3.6H_2O$ was dissolved in 20 mL of water in a 100 mL flask and the solution was heated to 100°C. Then, 12.5 mmol (2.07 g) 1,4-BDC suspended in 6ml of 2 M NaOH was added to the flask under stirring. The mixture was then refluxed for 12 hours at 120°C. After that a colourless gel was filtered and washed with 30 ml of water. The sample was then dried overnight under air. The free BDC linker present in the as-synthesized product was removed via calcination under air at 340°C.

Activation procedure:

The as synthesized powder was finely grinded and well spread in a watch glass. The watch glass was then placed inside a programmable furnace. The sample was heated to 340 °C (with a 2 hours ramp) and held at 340 °C for 30 hours. After cooling to room temperature, the powder was collected and characterized using PXRD TGA and IR.

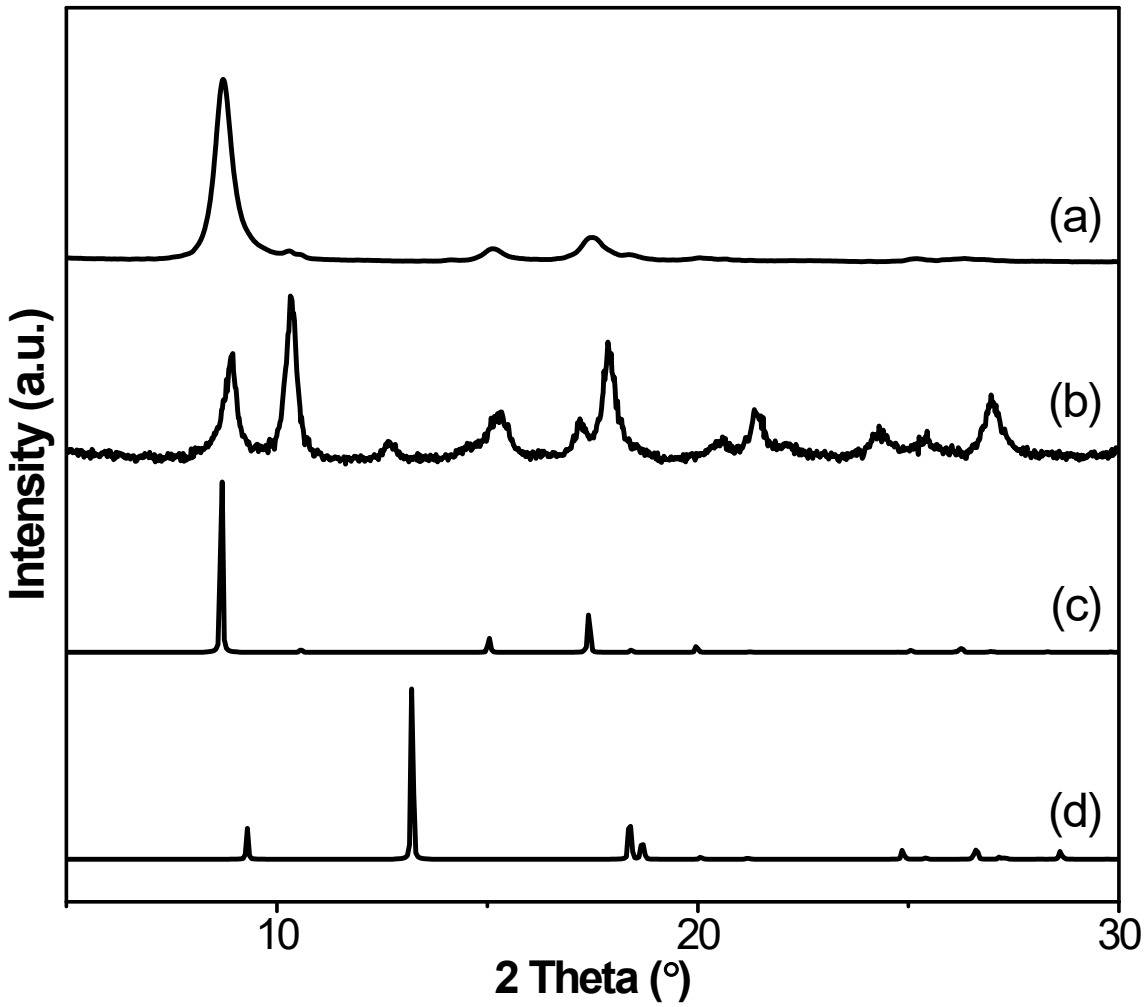

Figure S22 - Experimental PXRD pattern of non-functionalized a) MIL-53(Al) as synthesized and b) calcinated compared with calculated patterns of the two different pores configuration, c) Large pore (LP) and d) narrow pore (NP) (CuKα radiation, λ = 1.5418 Å).[11]

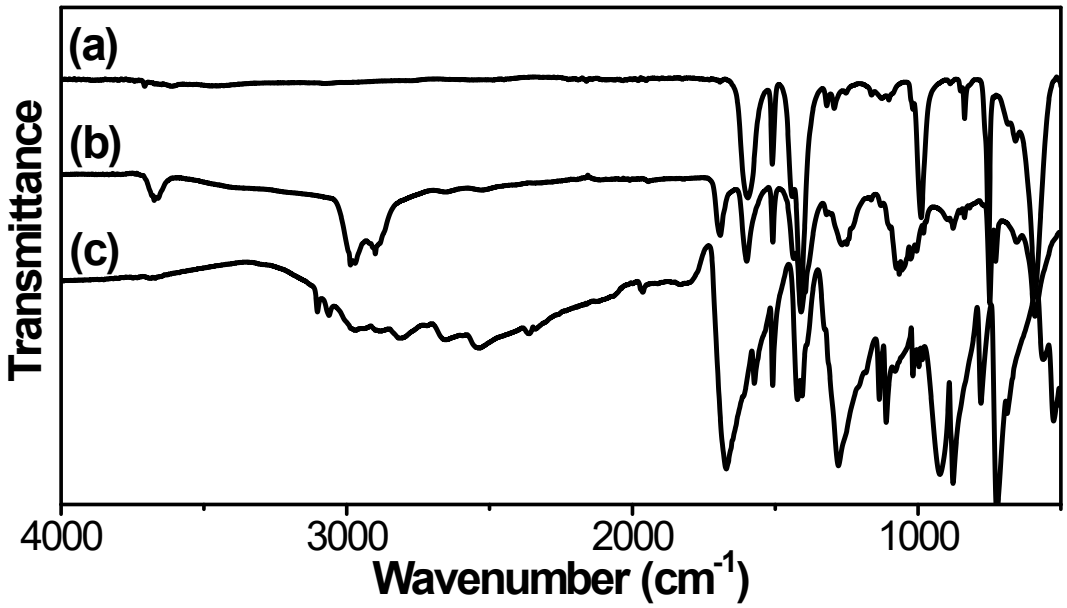

Figure S23 - Transmission IR spectrum of non-functionalized MIL-53(Al) a) calcinated, b) as synthesized compared with the c) linker spectrum.

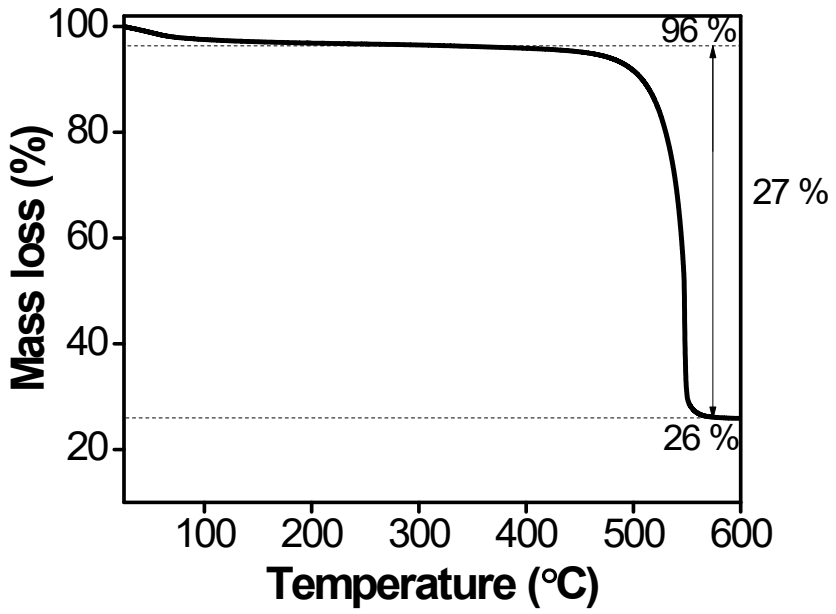

Figure S24 - TGA curve (3°C per min under O_2) of non-functionalized MIL-53(Al).

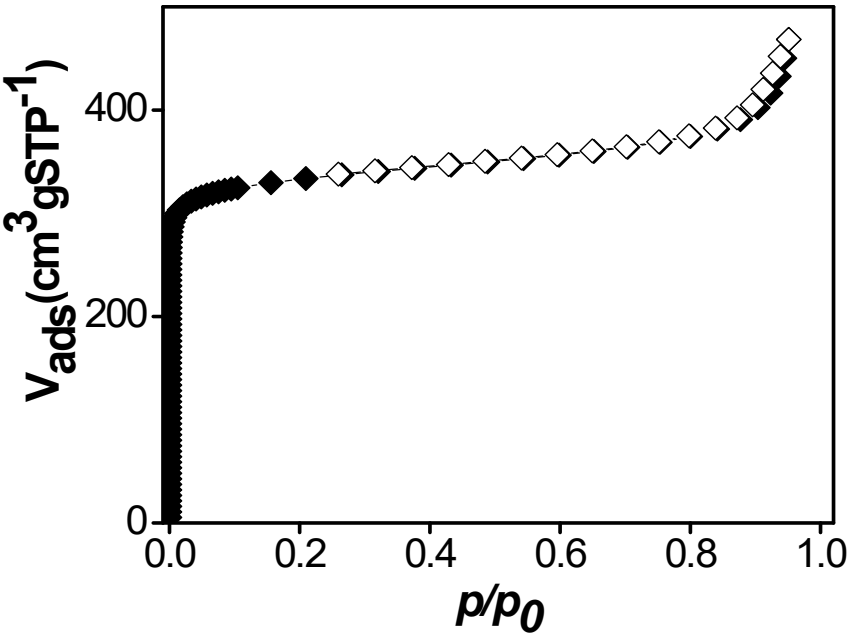

Figure S25 - Nitrogen adsorption isotherms, at 77K, of non-activated MIL-53(Al).

N_2 sorption isotherm is presented in Figure S25, the Brunauer–Emmett–Teller (BET) surface area of non-functionalized MIL-53(Al) was calculated to be 1325 $m^2 g^{-1}$, and with a pore volume of around 0.48 $cm^3 g^{-1}$, in agreement with values from the literature for a MIL-53(Al) obtained with DMF extraction.[11]

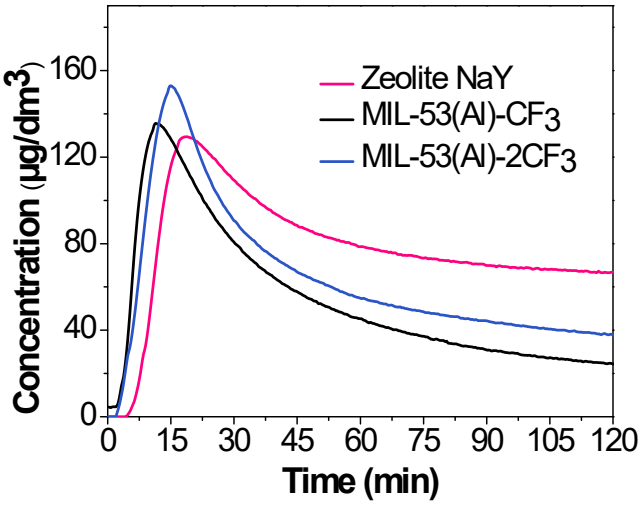

Figure S26 - Acetic acid concentration profiles inside a closed chamber after the injection of 1 µL of acetic acid at 25 °C and 40 %R.H., of MIL-53(Al)-$2CF_3$ and zeolite NaY compared with MIL-53(Al)-CF_3.

2. *Interaction energy and accessible volume determination based on single component isotherms*

The adsorption affinity towards methanol and hexane resulted in an expected decrease in uptake compared with the non-functionalized structure.[12], [13] The adsorbed amount (n_{ads}) in each case was converted to liquid-like volume and the analysis of the adsorption isotherms was made using Dubinin-Astakhov (D-A) equation equation[14].. A comparison with the nitrogen adsorption is done to better asses the porous volume that is accessible to that vapour in terms of the available microporous volume. In the D-A equation the amount adsorbed (cm^3 vapor per gram of MOF) is expressed as:

$$w = w_0 \exp\left(-(A/E)^n\right) \quad (6)$$

Where, w_0 is the limiting adsorbed volume, A is the adsorption potential ($A = RTln(p_0/p)$), E and n are temperature-independent parameters. E is the characteristic adsorption energy for a reference vapor[15]. As can be seen (Table 1) from the w_0 values in each vapor case, the total micropore volume obtained by N_2 is accessible to the VOCs with a percentage ranging from 73% (acetic acid) to 85% (acetaldehyde and acetone). Water exhibited the lowest w_0 value of 68% at p/p_0 close to 1. It is important to note that the region of interest of the studied vapors lies in the low concentration region while that for water is in the p/p_0 = 0.4-0.6 region. For the studied vapors the desired steep uptake is measured at very low p/p^0 values, while for water an uptake increase is observed only starting from p/p_0 of 0.7.

Table S4 shows the D-A equation parameters for the studied vapors along with 95% confidence bounds. Non-linear least squares method was used with Levenberg-Marquardt algorithm to fit the isotherms using equation (6) (shown in solid lines in Figure 5). The correlation coefficient ranged between 0.98 (nitrogen) to 0.9996 (acetaldehyde).

This study helps to better understand the adsorbent-adsorbate interaction that dictates each isotherm shape and reveals the excellent affinity of the MIL-53-CF_3 material towards several noxious VOCs in clear contrast with its hydrophobicity.

Table S4 - D-A equation parameters for the studied vapors along with 95% confidence bounds. Non-linear least squares method was used with Levenberg-Marquardt algorithm to fit the isotherms using equation (6) (shown in solid lines in Figure 5). The correlation coefficient ranged between 0.98 (nitrogen) to 0.9996 (acetaldehyde).

Parameters	Acetic acid	Hexane	Acetone	Methanol	Acetald-ehyde	water	Nitrogen
W_0 (cm^3 g^{-1})	0.23 (0.22, 0.25)	0.248 (0.24, 0.25)	0.267 (0.26, 0.27)	0.266 (0.26, 0.27)	0.27 (0.24, 0.3)	0.22 (0.17, 0.26)	0.317 (0.31, 0.32)
E (kJ mol^{-1})	14.24 (13.73, 14.74)	14.61 (13.94, 15.28)	16.04 (15.55, 16.53)	6.98 (6.77, 7.19)	13.26 (12.72, 13.81)	0.84 (0.68, 1.00)	6.934 (6.744, 7.125)
n	3.71 (2.95, 4.48)	2.63 (2.25, 3.02)	1.99 (1.83, 2.14)	1.92 (1.73, 2.11)	2.55 (2.35, 2.76)	1.21 (0.92, 1.51)	2.145 (1.917, 2.373)

[1] P. Giannozzi *et al.*, "A Modular and Open-Source Software Project for Quantum Simulations of Materials," *J. Phys. Condens. Matter*, vol. 21, no. 39, p. 395502, 2009.

[2] G. Makov and M. C. Payne, "Periodic Boundary Conditions in Ab Initio Calculations," *Phys. Rev. B*, vol. 51, no. 7, pp. 4014–4022, 1995.

[3] D. Vanderbilt, "Soft self-consistent pseudopotentials in a generalized eigenvalue formalism," *Phys. Rev. B*, vol. 41, no. 11, pp. 7892–7895, 1990, doi: 10.1103/PhysRevB.41.7892.

[4] S. Grimme, "Semiempirical GGA-type density functional constructed with a long-range dispersion correction," *J. Comput. Chem.*, vol. 27, no. 15, pp. 1787–1799, Nov. 2006, doi: 10.1002/jcc.20495.

[5] R. Serna-Guerrero and A. Sayari, "Modeling adsorption of CO2 on amine-functionalized mesoporous silica. 2: Kinetics and breakthrough curves," *Chem. Eng. J.*, vol. 161, no. 1–2, pp. 182–190, 2010, doi: 10.1016/j.cej.2010.04.042.

[6] A. K. Rappé, C. J. Casewit, K. S. Colwell, W. A. Goddard, and W. M. Skiff, "UFF, a Full Periodic Table Force Field for Molecular Mechanics and Molecular Dynamics Simulations," *J. Am. Chem. Soc.*, vol. 114, no. 25, pp. 10024–10035, 1992, doi: 10.1021/ja00051a040.

[7] S. L. Mayo, B. D. Olafson, W. a G. Iii, E. Eb, E. a E. T. El, and W. A. Goddard, "DREIDING: A generic force field for molecular simulations," *J. Phys. Chem.*, vol. 94, no. Suite 540, pp. 8897–8909, 1990, doi: 10.1021/j100389a010.

[8] C. Campañá, B. Mussard, and T. K. Woo, "Electrostatic Potential Derived Atomic Charges for Periodic Systems Using a Modified Error Functional," *J. Chem. Theory Comput.*, vol. 5, no. 10, pp. 2866–2878, Oct. 2009, doi: 10.1021/ct9003405.

[9] G. Kamath, F. Cao, and J. J. Potoff, "An improved force field for the prediction of the vapor-liquid equilibria for carboxylic acids," *J. Phys. Chem. B*, vol. 108, no. 37, pp. 14130–14136, 2004, doi: 10.1021/jp048581s.

[10] A. J. Cruz, J. Pires, A. P. Carvalho, and M. B. De Carvalho, "Adsorption of Acetic Acid by Activated Carbons, Zeolites, and Other Adsorbent Materials Related with the Preventive Conservation of Lead Objects in Museum Showcases," vol. 49, pp. 725–

731, 2004, doi: 10.1021/je034273w.

[11] Y. Liu, J. H. Her, A. Dailly, A. J. Ramirez-Cuesta, D. A. Neumann, and C. M. Brown, "Reversible structural transition in MIL-53 with large temperature hysteresis," *J. Am. Chem. Soc.*, vol. 130, no. 35, pp. 11813–11818, 2008, doi: 10.1021/ja803669w.

[12] L. Feng *et al.*, "Common but differentiated flexible MIL-53(Al): role of metal sources in synthetic protocol for tuning the adsorption characteristics," *J. Mater. Sci.*, vol. 54, no. 8, pp. 6174–6185, 2019, doi: 10.1007/s10853-018-03287-6.

[13] G. A. González-Martínez *et al.*, "Confinement of alcohols to enhance CO2 capture in MIL-53(Al)," *RSC Adv.*, vol. 7, no. 40, pp. 24833–24840, 2017, doi: 10.1039/c7ra03608f.

[14] J. Pires, M. Pinto, A. Carvalho, and M. Brotas de Carvalho, "Adsorption of acetone, methyl ethyl ketone, 1,1,1-trichloroethane, and trichloroethylene in granular activated carbons," *J. Chem. Eng. Data*, vol. 48, no. 2, pp. 416–420, 2003, doi: 10.1021/je020180n.

[15] M. Jaroniec and R. Madey, "Physical interpretation of the energy parameter in the Dubinin-Raduskevich equation," *Carbon N. Y.*, vol. 26, no. 1, pp. 107–108, 1988, doi: 10.1016/0008-6223(88)90019-X.